Journal of Applied Mechanics and Technical Physics, Vol. 42, No. 4, pp. 589–595, 2001

EXPERIMENTAL INVESTIGATION OF STABILITY OF A HYPERSONIC BOUNDARY LAYER ON A CONE–FLARE MODEL

A. N. Shiplyuk

UDC 532.526

Stability of a hypersonic flow in the regions of laminar separation of the boundary layer on a cone–flare model is experimentally studied for a Mach number M = 5.92. *Development of natural disturbances and artificial wave packets in the boundary layer and separation region is examined. It is shown that high-frequency disturbances are predominantly amplified in the separation region; the most unstable waves are those propagating with an angle close to* 60° *to the free-stream direction. It is found that separation and reattachment lines are generators of two-dimensional disturbances.*

Introduction. Hypersonic flow around flying vehicles is accompanied by the formation of intense shock waves, which are formed not only on the front part of the fuselage and on the leading edge of the wing but also on deflected control surfaces, compression surfaces of inlets, etc. Shock waves may interact with the boundary layer on the aircraft surfaces. A large positive pressure gradient arising thereby exerts a significant effect on the structure and characteristics of the boundary layer and may cause the emergence of laminar separation regions. Therefore, it is of interest to study the influence of laminar separation on instability and transition in the hypersonic boundary layer. In addition, the action of pressure gradients determined by the surface shape on the development of instability allows a passive control of the boundary layer. The available experimental works deal mainly with shock wave–boundary layer interaction and also with the effect of the pressure gradient on the mean flow in laminar, transitional, and turbulent regimes.

The effect of pressure gradient on stability of a compressible boundary layer was numerically studied by Malik [1]. It was found that a favorable pressure gradient exerts a stabilizing action on second-mode disturbances. This effect is manifested in a decrease in the maximum value of the growth rate and its shift to the region of higher frequencies, which leads to a decrease in the frequency range of growing disturbances. The effect of favorable and adverse pressure gradients on stability of a compressible boundary layer was theoretically examined by Zurigat et al. [2]. It was shown, in particular, that the efficiency of using the favorable pressure gradient for laminar-flow control decreases at hypersonic Mach numbers. In addition, three-dimensional first-mode disturbances are much more unstable in the presence of an adverse pressure gradient than two-dimensional first-mode waves.

A supersonic boundary layer on a cone model with a compression angle was experimentally studied by Kosinov and Shevelkov [3] for M = 2. Under conditions of laminar separation by the method of artificial wave packets, it was shown that the wave amplitude increases actually for all angles between the waves and the flow direction. The maximum growth was observed for greater angles of inclination, as compared to the case of a cone without a compression angle.

An analysis of the results of [4], where the Görtler vortices formed by incidence of a shock wave on a laminar boundary layer were observed, shows that one has to study more carefully the characteristics of disturbances and to clarify which disturbances, developing, lead to the laminar–turbulent transition.

The measurement of natural disturbance spectra only does not allow one to separate disturbances present in the boundary layer and to study the characteristics of individual disturbances. This hinders the comparison of experimental and numerical data. Spatial characteristics of disturbances in a hypersonic boundary layer, which

Institute of Theoretical and Applied Mechanics, Siberian Division, Russian Academy of Sciences, Novosibirsk 630090. Translated from Prikladnaya Mekhanika i Tekhnicheskaya Fizika, Vol. 42, No. 4, pp. 31–39, July–August, 2001. Original article submitted June 26, 2000; revision submitted December 25, 2000.

0021-8944/01/4204-0589 $25.00

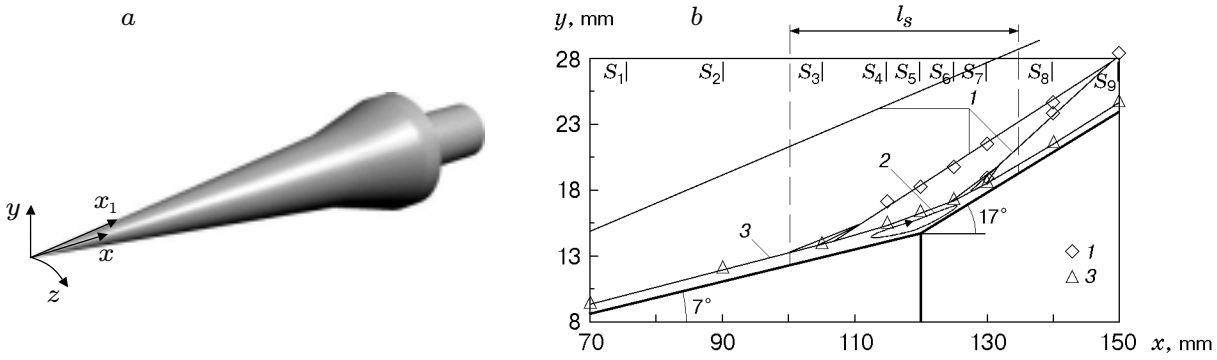

Fig. 1. Scheme of the model (a) and flow pattern (b): 1) shock waves; 2) separation region; 3) boundary-layer edge.

were obtained using correlation measurements, were studied in [5, 6]. A more preferable method for stability studies is the method of artificial wave packets, which was developed at the Institute of Theoretical and Applied Mechanics (ITAM) of the Siberian Division of the Russian Academy of Sciences for a supersonic boundary layer [7]. This method is used in the present work to study the spatial structure of disturbances in a hypersonic boundary layer.

Present work is a continuation of experimental studies of the characteristics of a hypersonic flow on a cone–flare model [8]. A cone model with a 7° apex half-angle and a 10° compression angle was used to study the mean flow structure and to measure the mean and fluctuating characteristics of the boundary layer in the vicinity of the separation region for a Mach number $M_\infty = 5.92$ and a unit Reynolds number $Re_1 \simeq 12.5 \cdot 10^6$ m^{-1}. The model dimensions and geometry and the flow pattern are shown in Fig. 1 (l_s is the separation-region length). A laminar separation of the boundary layer is formed on this model for the above flow parameters. As the flow crosses the line of reattachment, the character of variation of the mean parameters of the boundary-layer flow indicates the beginning of flow turbulization. The main share of energy of disturbances in the boundary layer and in the shear layer above the separation region is concentrated in a narrow band located near the upper boundary of the viscous layer. It is shown that separation strongly decreases the stability of the laminar flow and leads to rapid turbulization of the latter. Propagation of artificial wave packets in such a flow is studied in the present work. Detailed information on the characteristics and development of individual waves in the disturbance spectrum is obtained and compared with the measurement results for natural disturbances.

Experimental Setup. The experiments were conducted in a T-326 hypersonic wind tunnel based at ITAM. The flow characteristics corresponded to the conditions of [8] ($M_\infty = 5.92$, $T_0 = 390$ K, $P_0 = 1.01$ MPa, and $Re_1 = 12.5 \cdot 10^6$ m^{-1}). The T-326 wind tunnel is a free-jet setup with exhaustion to the atmosphere [9]. The running time of the wind tunnel is determined by the operation regime and reaches 20 min when the nozzle designed for M = 6 is mounted. The test section of the T-326 wind tunnel is a free-jet chamber; the flow-core diameter is 180 mm. To avoid condensation, the air was heated by an electric heater. Under the present test conditions, the nonuniformity of the velocity field was less than 0.7%. During each experiment, the pressure P_0 and the temperature T_0 in the plenum chamber were measured and sustained constant within 0.5%. The level of mass-flow fluctuations under the present test conditions was approximately 1%.

The T-326 wind tunnel is equipped by a three-component traversing gear, which moves a one-component microtraversing gear with a gauge mounted on it (a hot-wire probe or a Pitot tube). The error of traversing-gear mounting is 0.1 mm in the x, y, and z directions. The microtraversing gear serves to move the probe in the boundary layer along the normal to the model surface with an accuracy of 0.01 mm. To facilitate wind-tunnel starting and to avoid destruction of the probes by unsteady loads, the model and traversing gears together with the probe were inserted into the wind tunnel after its starting.

Model. The model is a cone with a 7° apex half-angle and a 17° flare angle (Fig. 1). The length of the nose cone is 120 mm, the length of the flare is 33.6 mm, and the total length of the model is 165.6 mm. The bluntness radius of the model tip was less than 0.01 mm. The error of model mounting in terms of the angles of attack and sideslip was 0.06 and 0.03°, respectively [8]. The model was equipped by a generator of artificial disturbances, which was placed inside the model at a distance of 60 mm from the nose tip. The source of disturbances was a high-frequency glowing electric discharge. The construction of the source is similar to that described in [7]. The disturbances were introduced into the boundary layer from a discharge chamber through an orifice 0.4 mm

in diameter on the model surface. The source of disturbances was fed by a generator, which produced a variable sinusoidal voltage with an amplitude up to 1000 V. In the course of an experiment, the amplitude of voltage oscillations on the electrodes was sustained constant, which was ensured by stabilization of the power feeding the generator [10]. Rotation of the model around the longitudinal axis by a mechanism that ensured an error of rotation less than 0.1° allowed us to study the evolution of an artificial wave packet in the transverse direction.

Measurement Techniques. To study the evolution of natural and artificial disturbances in the boundary layer, we used a constant-current hot-wire anemometer TPT-4 manufactured at ITAM. The use of tungsten-wire probes 5 μm in diameter and 1.3 mm long ensured operation of the hot-wire anemometer with a frequency up to 200 kHz. The hot-wire probe location relative to the model surface was determined by the electric contact after model insertion into the flow, after which the probe was temporarily switched off from the hot-wire anemometer. When the distributions of the mean and fluctuating characteristics were measured across the boundary layer, the probe moved in a direction from the model wall with a step of 0.05 mm.

In the course of experiments, the variable and constant electric signals from the hot-wire output were digitized by a two-channel 10-bit analog-to-digital converter and were fed into the memory of a personal computer. In studying natural disturbances, 400 instantiations with 512 records were registered at each point. For obtaining oscillation spectra, the variable signal from the hot-wire anemometer was digitized with a frequency of 333 kHz, which allowed a spectral analysis within a frequency range of 650–$166 \cdot 10^3$ Hz with a resolution of 650 Hz. To avoid the possible spurious effect of signals with a higher frequency, a low-frequency filter was used, which cut off signals with frequencies higher than $166 \cdot 10^3$ Hz. The noise of the constant-current hot-wire anemometer was determined as follows: feeding of the measurement bridge was switched off, and the signal at the hot-wire output was measured, which is the electronic noise. Since flow oscillations and hot-wire noise are not correlated, the noise was subtracted from the measured signal as a random quantity.

In experiments with artificial disturbances, the variable signal of the hot-wire anemometer passed through a narrow-band filter with a transmission band of 1%, which was tuned to the frequency of the source of disturbances. The signal-to-noise ratio significantly improved, since the 1% transmission band corresponds to averaging of 100 period of oscillations. The variable and constant components of the hot-wire signal were digitized with a frequency of 1 MHz. To eliminate random fluctuations and identify the signal of artificial disturbances, the time oscillograms were processed by the method of simultaneous averaging over an ensemble. For this purpose, the oscillograms (256 records) were registered simultaneously with ignition of the electric discharge and were summed 1000 times. The use of this method allowed us to increase multiply the signal-to-noise ratio and to separate the signal from the artificial disturbance despite its low amplitude.

Data Processing. The constant-current hot-wire anemometer is widely used in supersonic flow studies. It is known that mass-flow fluctuations in a supersonic boundary layer are much greater than the stagnation temperature fluctuations, and the sensitivity coefficients for the mass flow F and stagnation temperature are approximately of the same order for the overheating using in this work $a_w = 0.5$–0.8 [11]. Therefore, we may assume that the hot-wire probe is sensitive in this case only to mass-flow fluctuations. In determining these fluctuations, we used the results of [12]. The procedure of processing of the measurement results is described in detail in [13].

In determining the amplitude A and phase Φ of artificial disturbances in the course of experiments, a discrete Fourier transform of the averaged time oscillograms of mass-flow fluctuations m was performed:

$$A(x,z)\mathrm{e}^{i\Phi(x,y,z)} = \frac{2}{N}\sum_{j=1}^{N} m(x,z,t_j)\mathrm{e}^{-i\omega t_j}.$$

The spectra with respect to the transverse wavenumber β were obtained using a discrete Fourier analysis

$$A(\beta)\mathrm{e}^{i\varphi(\beta)} = \int\limits_{-z_0}^{z_0} A(z)\mathrm{e}^{i\varphi(z)}\mathrm{e}^{-i\beta z}\,dz,$$

where z_0 is the transverse coordinate corresponding to the wave-packet boundary.

Since the flow examined is rather complicated and the number of cross sections considered is limited, it does not seem possible to perform a complete spectral analysis in the longitudinal direction. A simplified technique was used to obtain phase velocities of waves with different angles of inclination. The phase was measured linearly along x for all β; therefore, the streamwise wavenumber α_r was found by linear approximation of the dependence $\varphi(x,\beta) = \alpha_r(\beta)x + C$. The normalized phase velocity of disturbances was determined as $C_x(\chi) = \lambda f/U_e$, where

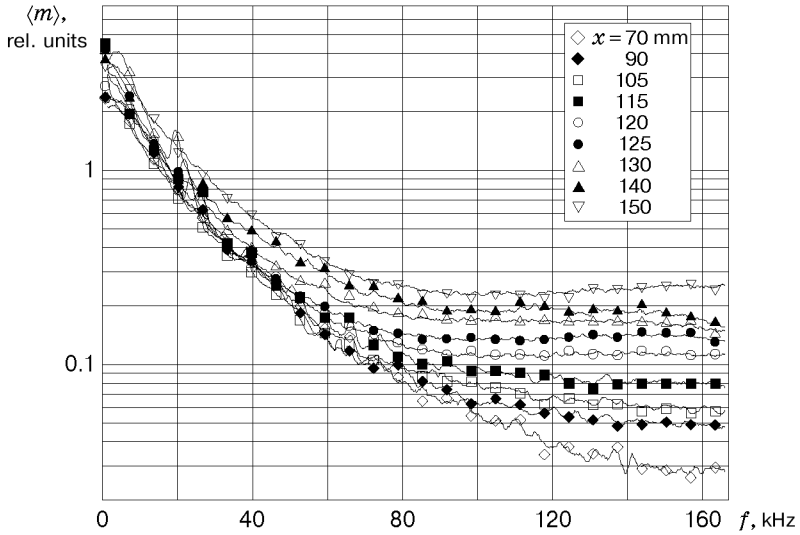

Fig. 2. Spectra of natural disturbances in the maxima of oscillations.

$\chi = \arctan(\beta/\alpha_r)$ is the angle between the wave vector and the main-flow direction, U_e is the velocity at the boundary-layer edge, and $\lambda = 2\pi/\alpha_r$ is the disturbance wavelength. It should be noted that these estimates have an integral character, and only approximate conclusions on the wave-packet structure may be drawn.

Measurement Results for Natural Disturbances. The characteristics of natural oscillations were measured at their maxima located at the external boundary of the shear layer, in cross sections S_1–S_9 (Fig. 1). The positions of the measurement cross sections were chosen in [8]. Profiles of velocity and integral oscillations were obtained for these cross sections. Figure 2 shows the spectra $\langle m \rangle$ within the frequency range of 650–$166 \cdot 10^3$ Hz for nine cross sections, which were measured in the maxima of oscillations. In accordance with the character of the dependence obtained, the oscillations may be divided into three regions: low-frequency (less than 20 kHz), medium-frequency (20–80 kHz), and high-frequency (more than 80 kHz) regions. Low-frequency oscillations in the separation region increase insignificantly (approximately by a factor of 1.5). Oscillations in the range of medium frequencies remain almost unchanged. High-frequency oscillations in the separation region increase significantly (approximately by a factor of 5). The boundary between the medium-frequency and high-frequency oscillations is not constant and moves gradually to the region of lower frequencies. After flow reattachment ($x = 140$ and 150 mm), oscillations of all frequencies increase, and the vertical profiles of integral oscillations become more filled [8], which indicates the beginning of boundary-layer turbulization. Figure 2 shows that the fraction of high-frequency disturbances is small, and the profiles of integral oscillations obtained in [8] are mainly determined by the intensity of low-frequency oscillations.

Artificial Wave Packets. As it follows from the results of studying the evolution of natural disturbances [8] and from the data of other works (see, for example, [14]), the main energy of oscillations in a hypersonic boundary layer is concentrated in a narrow region near the upper edge of the boundary layer (the so-called critical layer). Therefore, spatial distributions of the characteristics of natural disturbances were studied only in a vicinity of this layer. In each cross section, the probe was mounted at a distance from the wall corresponding to the maximum value of the variable component of the hot-wire signal. Then the model was rotated around the longitudinal axis with a step of 3°, and the distributions of the signal amplitude and phase were recorded as functions of the angle of model rotation θ. Thus, distributions of disturbance amplitudes and phases along the transverse coordinate z were obtained in nine cross sections. The close distance between the cross section S_1 ($x = 70$ mm) and the source of disturbances located at a distance $x = 60$ mm did not allow measurements with an acceptable accuracy because of the large level of electric induction on the hot-wire probe from the electric discharge in the power source. Therefore, the data were obtained in the cross section S_1' ($x = 76$ mm).

Artificial disturbances were introduced at a frequency of 40 kHz, which, according to the measurement results of the spectra of natural disturbances, corresponds to the range of medium frequencies of natural disturbances (20–80 kHz). The running time of the T-326 wind tunnel did not allow investigations in all cross sections during one run; therefore, the measurements were performed in two stages: in cross sections S_1–S_5 and S_5–S_9. Because

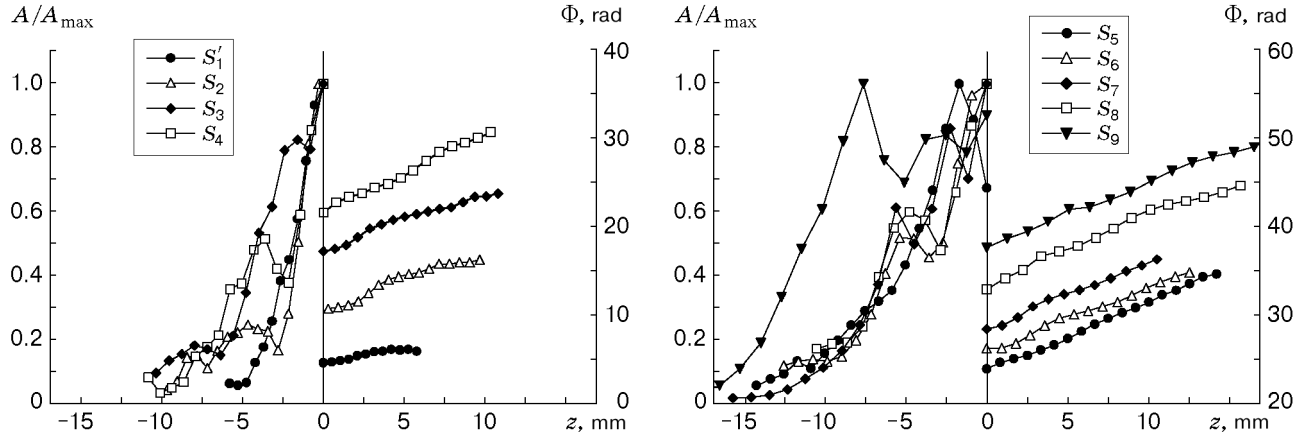

Fig. 3. Transverse distributions of the amplitudes and phases of artificial disturbances.

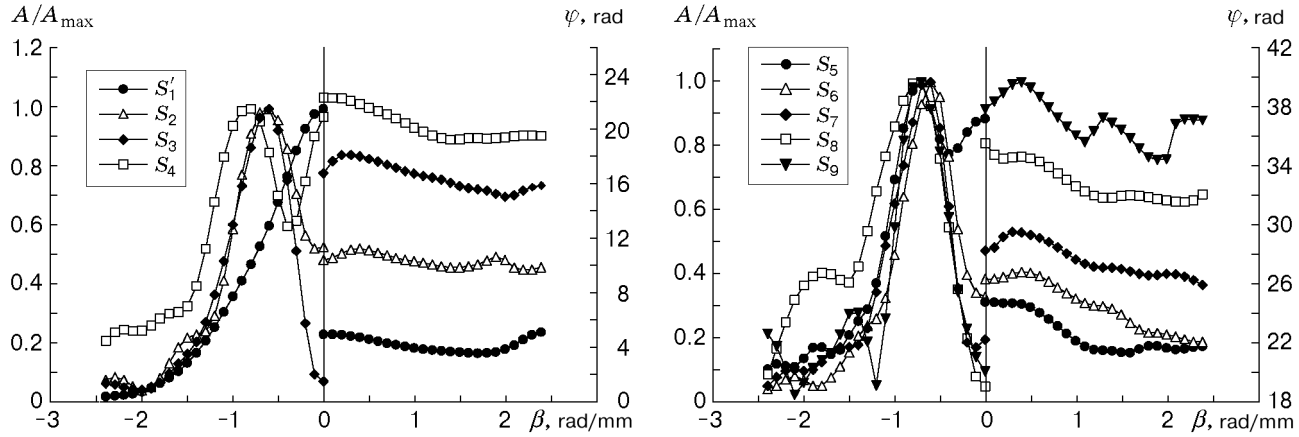

Fig. 4. Amplitude and phase spectra of artificial disturbances.

of the limited running time of the wind tunnel, the measurements were performed within the range of model rotation angles $-5^\circ < \theta < \theta_0$. The results of data processing for the amplitude and phase distributions were made symmetric relative to the angle θ. The angle θ was counted from the generatrix at which the orifice of the source of disturbances was located. It follows from the measurement results within the range of angles $-\theta_0 < \theta < \theta_0$ that the transverse distributions of the amplitude and phase in the wave packet are almost symmetric, and the procedure of symmetrization does not introduce any significant error into the results of data processing. The value of θ_0 was found from the condition $A_{\theta_0} = 0.03A_{\max}$. For the spectral analysis in terms of β, the distributions of the amplitude $A(\theta)$ and phase $\Phi(\theta)$ were recalculated to the dependences $A(z)$ and $\Phi(z)$, where z is the transverse coordinate counted along the line of relative motion of the probe ($z_{\theta=0} = 0$). It was found in preliminary measurements that the mean and fluctuating voltages at the hot-wire probe are independent of the transverse coordinate, i.e., there are no streamwise vortices, such as the Görtler vortices, in this cross section.

It should be noted that it is not possible to determine the boundary of the wave packet in cross sections S_4–S_7 using the above criterion of the low amplitude. This may be attributed to the presence of the separation region and rather complicated character of evolution of disturbances inside it. The oscillations become chaotic in these cross sections as the wave-packet boundary is approached. In conducting the spectral analysis in terms of transverse wavenumbers, the wave-packet boundary in these cross sections was determined from the condition of a smooth distribution of the signal phase along z. This assumption did not introduce any significant error in data processing, since the amplitude of oscillations at the wave-packet boundary was much lower than in the center.

Since the source of disturbances could not operate continuously, it was switched off for the time of probe displacement from one cross section to another. Because of this, the reproduction of the amplitudes of introduced disturbances could not be guaranteed in measurements in different cross sections. Therefore, the amplitude distri-

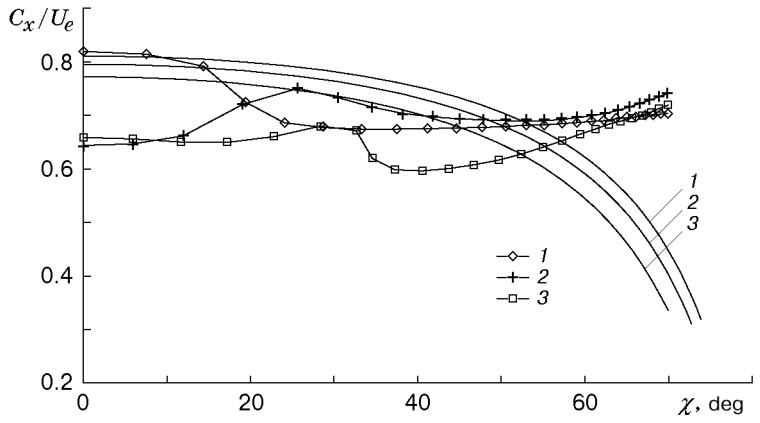

Fig. 5. Normalized longitudinal phase velocity C_x/U_e of artificial disturbances versus the angle of inclination of the wave vector χ for three flow regions: upstream of separation (1), in the separation region (2), and downstream of reattachment (3); the solid curves show the calculations by the formula $C_x/U_e = 1 - 1/(\mathrm{M}_e \cos\chi)$; the points are the measurement results.

bution in each cross section was normalized to the corresponding maximum value $A_{\max}$. The distributions of the normalized amplitudes and phases of artificial disturbances over the transverse coordinate z are plotted in Fig. 3. (Because of the symmetry, Figs. 3 and 4 show the amplitude distributions only for negative values of z and phase distributions only for positive values.) It is seen that inclined waves prevail in the wave packet, and the angle of inclination increases downstream.

The spatial amplitude and phase spectra as functions of the transverse wavenumber β were calculated for all cross sections, using the technique described above. The distributions obtained are plotted in Fig. 4. It is seen that the source generates a wave packet with a large fraction of waves with small angles of inclination. Then the two-dimensional wave ($\beta \approx 0$) rapidly decays, and inclined waves start to play the major role. The wave propagating at an angle close to 60° ($\beta \simeq 0.7$) starts to dominate already in the second cross section and can be found in wave spectra of all subsequent cross sections. It should be noted that the plane wave appears again in the wave spectrum in the cross section S_4 located immediately behind the separation line. This testifies that the separation circumference is a generator of two-dimensional disturbances. In the course of evolution of the wave packet in the shear flow above the separation region, the plane wave rapidly decays, and waves with an angle of inclination close to 60° start to prevail again. For cross sections located behind the reattachment line, the amplitude spectra have a peak, which corresponds to a wave propagating at an angle close to 75°. An increase in the amplitude of waves with considerable angles of inclination is typical of subharmonic resonance at the stage of nonlinear interaction of disturbances [15]. Destruction of the wave packet is observed in the cross section S_9, which is evidenced by the appearance of additional peaks in the amplitude and phase spectra.

Figure 5 shows the dependence of the normalized longitudinal phase velocity of disturbances C_x/U_e on χ for three flow regions: upstream of separation, in the separation region, and downstream of reattachment. The values of velocity at the boundary-layer edge U_e obtained in [8] were used for normalization. The points refer to the measurement results and solid curves refer to the maximum velocity of propagation of acoustic disturbances versus the angle of inclination of the wave vector $C_x/U_e = 1 - 1/(\mathrm{M}_e \cos\chi)$. According to the linear theory of stability, acoustic disturbances with longitudinal phase velocities lying above these curves cannot exist.

The limited number of experimental cross sections in the streamwise direction did not allow a spatial spectral analysis in this direction. Therefore, Fig. 5 shows the averaged dependences of the phase velocity of disturbances present in the flow, both vortex and acoustic ones, on χ. Correspondingly, the angles of wave inclination χ were determined from the values of α_r calculated by the dependences $C_x(\beta)$. The difference in phase velocities of acoustic and vortex waves (Fig. 5) is indicative of their presence in the wave packet. The Tollmien–Schlichting waves prevail close to the source at small ($\chi < 10°$) and large ($\chi > 55°$) angles of inclination; acoustic waves dominate at angles $10° < \chi < 55°$. Acoustic waves also prevail in the separation region and downstream of flow reattachment within the entire range of angles up to $\chi = 55°$. The fraction of these waves increases significantly at small angles of inclination ($\chi < 20°$), whereas the fraction of Tollmien–Schlichting waves increases within the range of angles $20° < \chi < 55°$. The longitudinal phase velocity of waves with angles $\chi > 55°$ remains practically unchanged.

Conclusions. It is shown that the growth of natural disturbances of the boundary layer depends on frequency. Disturbances with frequencies higher than 80 kHz are most unstable. No streamwise vortices were found in the flow examined.

In the case of artificially introduced disturbances with a frequency of 40 kHz, waves with a 60° angle of inclination are most unstable. It was found that lines of flow separation and reattachment are generators of two-dimensional disturbances. Acoustic disturbances dominate within the range of angles of wave inclination smaller than 55°, whereas disturbances of the vortex nature prevail at large angles of inclination.

This work was supported by Aerospatiale (Contract No. 239.337) and the Russian Foundation for Fundamental Research (Grant No. 98-01-00735).

REFERENCES

1. M. R. Malik, "Prediction and control of transition in hypersonic boundary layers," AIAA Paper No. 87-1414, New York (1987).
2. Y. H. Zurigat, A. H. Nayfeh, and J. A. Masad, "Effect of pressure gradient on the stability of compressible boundary layers," AIAA Paper No. 90-1451, New York (1990).
3. A. D. Kosinov and S. G. Shevelkov, "Experimental investigation of separation and stability of supersonic laminar boundary layer," in:*Proc. of the IUTAM Symp. on Separated Flows and Jets* (Novosibirsk, USSR, July 9–13, 1990), Springer-Verlag, Berlin–Heidelberg (1991), pp. 741–745.
4. A. Henckels, A. F. Kreins, and F. Maurer, "Experimental investigation of hypersonic shock-boundary layer interaction," *Z. Flugwiss. Weltraumförsch.*, No. 17, 177–124 (1993).
5. R. Kimmel, A. Demetriades, and J. Donaldson, "Space–time correlation measurements in a hypersonic transitional boundary layer," AIAA Paper No. 95-2292, New York (1995).
6. A. A. Maslov, S. G. Mironov, and A. N. Shiplyuk, "Wave processes in a hypersonic shock layer on a flat plate," *Izv. Ross. Akad. Nauk, Mekh. Zhidk. Gaza*, No. 5, 162–168 (1998).
7. A. D. Kosinov, A. A. Maslov, and S. G. Shevelkov, "Experiments on the stability of supersonic laminar boundary layers," *J. Fluid Mech.*, **219**, 621–633 (1990).
8. A. N. Shiplyuk, "Experimental investigation of laminar separation on a cone–flare model at hypersonic velocities," *Teplofiz. Aeromekh.* (in press).
9. V. D. Grigor'ev, G. P. Klemenkov, A. I. Pirogov, and N. V. Yakovleva, "Hypersonic wind tunnel T-326 of ITAM. Methodical study of velocity and temperature fields," Report No. 1129, Inst. Theor. Appl. Mech., Sib. Div., Acad. of Sci. of the USSR, Novosibirsk (1980).
10. A. A. Maslov, A. A. Sidorenko, and A. N. Shiplyuk, "On an experimental technique for the study of hypersonic boundary layer stability," in: *Methods of Aerophysical Research*, Proc. of the Int. Conf. (Novosibirsk, Sept. 2–6, 1996), Vol. 2, Inst. Theor. Appl. Mech., Sib. Div., Russian Acad. of Sci., Novosibirsk (1996), pp. 175–179.
11. D. Bestion and J. Gavigilo, "Comparison between constant-current and constant-temperature anemometers in high speed flows," *Rev. Sci. Instrum.*, **54**, 1513–1524 (1983).
12. V. N. Zinov'ev and V. A. Lebiga, "Hot-wire measurements in compressible flows," *Izv. Akad. Nauk SSSR, Ser. Tekh. Nauk*, No. 5, 22–31 (1990).
13. A. A. Maslov, A. N. Shiplyuk, A. A. Sidorenko, and Ph. Tran, "Study related to hypersonic boundary layer stability on a cone with a flare," Preprint No. 16-97, Inst. Theor. Appl. Mech., Sib. Div., Russian Acad. of Sci., Novosibirsk (1997).
14. K. F. Stetson and R. L. Kimmel, "On hypersonic boundary layer stability," AIAA Paper No. 92-0737 (1992).
15. A. D. Kosinov, N. V. Semenov, S. G. Shevelkov, and O. I. Zinin, "Experiments of the nonlinear instability and transition using controlled disturbances," in: *Proc. of the IUTAM Symp. on Nonlinear Instability of Nonparallel Flows* (Potsdam, N.Y., U.S.A., July 26–31, 1993), Springer-Verlag, Berlin–Heidelberg (1994), pp. 196–205.